Development and Control of a Bioinspired Robotic Remora for Hitchhiking

Pengfei Zhang, Zhengxing Wu, Yan Meng, Huijie Dong, Min Tan, and Junzhi Yu, *Fellow, IEEE*

***Abstract*—Remora, a bony fish, is well known for the remarkable hitchhiking behavior, by which it can transport itself over large distances without too much effort. In this article, a novel robotic remora with a stable adhesion system and its motion control methods are proposed for transferring the hitchhiking behavior to the engineered system. In terms of the mechatronic design, a robotic prototype with the uncoupled planar and vertical motion mechanisms is created to realize the precise and agile movement. Furthermore, a reliable adhesion system possessing low preload demand, considerable adhesive force ($\sim$ 250 N), and reversible adhesion ability is developed, and then, the design principle of the adhesive disc is investigated. In the aspect of motion control, a mode-switch-based planar pose (position and orientation) control method and an antidisturbance depth control method are designed. The combination of these two controllers endows the robotic remora with the ability to precisely arrive at any position in a 3-D space, which paves the way for the hitchhiking task. Extensive experimental results are presented to support the performance benefits of the proposed robotic remora and control methods. Finally, the hitchhiking behavior is implemented successfully by robotic remora. To the best of our knowledge, this is the first engineered implementation of hitchhiking for a fin-actuated underwater robot. The results obtained will promote the design and control of the future underwater adhesion robot and offer valuable insights into the long-endurance robotic fish and mother–son multirobot system.**

***Index Terms*—Bioinspired adhesion, depth control, pose control, remora, robotic fish.**

Manuscript received 5 July 2021; revised 22 September 2021; accepted 5 October 2021. Date of publication 4 November 2021; date of current version 17 October 2022. Recommended by Technical Editor J. Marshall and Senior Editor K. Kyriakopoulos. This work was supported in part by the National Natural Science Foundation of China under Grants 61725305, 62033013, U1909206, 62022090, and 62073196, in part by the Beijing Nova Program under Grant Z201100006820078, and in part by the Youth Innovation Promotion Association of Chinese Academy of Sciences under Grant 2019138. *(Corresponding author: Junzhi Yu.)*

Pengfei Zhang, Zhengxing Wu, Yan Meng, Huijie Dong, and Min Tan are with the State Key Laboratory of Management and Control for Complex Systems, Institute of Automation, Chinese Academy of Sciences, Beijing 100190, China and also with the School of Artificial Intelligence, University of Chinese Academy of Sciences, Beijing 100049, China (e-mail: zhangpengfei2017@ia.ac.cn; zhengxing.wu@ia.ac.cn; mengyan2017@ia.ac.cn; donghuijie2018@ia.ac.cn; min.tan@ia.ac.cn).

Junzhi Yu is with the State Key Laboratory for Turbulence and Complex Systems, Department of Advanced Manufacturing and Robotics, Beijing Innovation Center for Engineering Science and Advanced Technology, College of Engineering, Peking University, Beijing 100871, China and also with the State Key Laboratory of Management and Control for Complex Systems, Institute of Automation, Chinese Academy of Sciences, Beijing 100190, China (e-mail: junzhi.yu@ia.ac.cn).

Color versions of one or more figures in this article are available at https://doi.org/10.1109/TMECH.2021.3119022.

Digital Object Identifier 10.1109/TMECH.2021.3119022

I. Introduction

OWING to high maneuverability, low drag, and low hydrodynamic noise, a fishlike robot has attracted significant interest over the past two decades, and a wealth of robotic fish prototypes have been developed [1]. However, due to the limitations on volume and payload, most robotic fishes are still confronted with the challenge of endurance time. In order to obtain longer endurance, the novel motion mechanism or the energy supplement scheme should be further studied [2]–[4].

Remora (family *Echeneidae*) is a special marine species that has a suction disc on the dorsal side, which receives attention owing to its remarkable hitchhiking behavior. As shown in Fig. 1, remora is capable to adhere to a broad range of hosts, including sharks, whales, mantas, turtles, and dolphins, to transport itself over large distances using its adhesive disc [5]. By means of this attachment ability, remora can take advantage of the increased probability of meeting conspecifics, lower predation risk, access to food such as the parasites on host, and especially the lower locomotor consumption. Studies have demonstrated that hitchhiking behavior can decrease oxygen consumption at 3.7–5.7% [6]. Namely, this hitchhiking behavior is an excellent way to reduce energy consumption and extend the battery endurance, which offers promising insight for the robotic fish design.

To realize the transfer of the hitchhiking behavior to the engineered system, two key technical problems are imperative to be addressed. First, a compact, practical, and reversible adhesive system with feedback, which can be mounted into a small robotic fish, is required to be designed. Second, 3-D position and attitude control of robotic fish is essential for approaching and attaching to the host [see Fig. 1]. Notably, when the robotic remora attempts to adhere to the undersurface of a horizontal suspending host, the desired roll, pitch angle, and velocity are zero. Thus, the 3-D control can be divided into two subproblems, including the planar pose (planar position and yaw) control and depth control. This article will focus on the solutions of adhesion system, planar pose control, and depth control.

The adhesive organs of animals exist widely in nature, e.g., gecko foot [7], and the sucker of octopus [8], clingfish [9], and remora [10]. However, for the aquatic environment, most adhesive organs on the terrestrial organisms will be invalid, and the negative pressure principle becomes the major adhesive mechanism. Suction disc is the most common adhesive organ

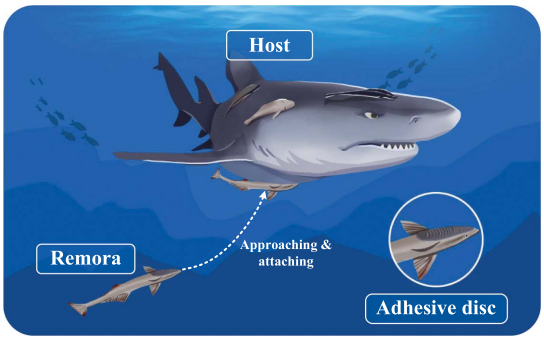

Fig. 1. Hitchhiking behavior of the remora suckerfish.

using the negative pressure principle, and thus, a number of biomimetic suckers have been developed, including the octopus-like sucker [11], the bionic tube feet of sea urchins [12], the bionic suction disc of clingfish [13], and the bioinspired remora sucker. Among these bionic suckers, the remora disc possesses the most complex interior structure and excellent adhesion performance. Wang *et al.* developed the first biomimetic remora disc and adopted soft actuator to mimic the functionality of lamellae and spinules of the real disc, which generates a considerable pull-off force and frictional force [14], [15]. Inspired by this research, the mechanism and material of adhesive disc were further studied for strengthening the adhesion performance [16], [17], but there are still two issues hindering the application of their suckers. First, a large preload is needed for creating a seal, and if the preload is not big enough, the adhesion performance will degrade enormously. Second, the perception ability of adhesive disc is missed, and thus, it cannot sense the adhesion status and whether a pressure leak exists or not.

Planar pose control is to regulate the robot position and orientation to desired values and decrease the robot velocity to zero simultaneously. Several attempts have been made in the planar pose control of robotic fish. One part of the previous studies realized the position and heading angle control, but was unable to guarantee that the velocity drops to zero [18]–[21]. The other part ensured the convergence of position and velocity, but the heading angle could not be controlled [22], [23]. In a word, these existing control methods cannot simultaneously realize the convergence of the position, orientation, and velocity for robotic fish. The major challenges are twofold. The first one is the underactuated characteristics, namely, the robotic fish cannot realize pivot steering and lateral motion. The second one is the complexity of the liquid environment. Owing to the low fluid drag and strong flow disturbance, it is hard to retain the position for robotic fish. Therefore, addressing these challenges on planar pose control is the focus of this article.

Depth control is to drive the robot to the desired depth and then maintain at that. The existing depth control methods for robotic fish can be divided into two classes according to the driving mechanism. The first category is adjusting the thrust direction of the fishtail, namely, the pitch angle, to realize the depth control, where the common actuators include pectoral fin [24], [25] and barycenter adjustment mechanism [26]. These methods usually have faster response speed but require the cooperation of the extra motion, like the flapping of the caudal fin. The second category is regulating the net buoyancy to change depth, where the common actuators include water injector [27], [28] and pump [29]. These methods require large space to store water but decouple the depth control from other motions. These mentioned methods have already achieved depth control in some scenes, but most of them do not take account of the impact of disturbance, e.g., the constant disturbance induced by the nonzero net buoyancy and the periodic disturbance caused by swimming. In this article, a buoyancy-driven depth controller considering the disturbance is studied.

This article aims to develop a feasible solution to mimic the hitchhiking behavior of the real remora. The main contributions are two folds. On the one hand, a novel robotic remora platform with a reliable adhesion system is developed for the first time, which successfully realizes the complete hitchhiking behavior on the surface of a remotely operated vehicle. The robotic remora possesses flexible mobility, especially the decoupled ability on planar and depth movement, which benefits from a pair of 360° pectoral fins and the buoyancy-driven system. The designed adhesion system exhibits superior characteristics compared with the previous adhesion schemes, including the low demand of preload, considerable pull-off ($\sim$ 250 N) and shear ($\sim$ 170 N) force, reversible adhesion, adhesion adaptability, and perceptual ability. On the other hand, a mode-switch-based planar pose controller and an antidisturbance depth controller of the robotic remora are designed to realize the adhesion task. Compared with the previous pose controllers, the proposed method can guarantee the convergence of position, heading angle, and velocity simultaneously. The designed depth controller takes account of the disturbance and possesses better control accuracy relative to traditional methods, including proportional–integral–derivative (PID) controller and feedback linearization method. Besides, since the proposed controllers mainly rely on the basic motion mode and universal fluid drag model rather than the specific robotic fish dynamics, the idea of pose and depth control can be easily applied for other underwater robots. In conclusion, this work successfully transfers the hitchhiking behavior into the engineered system, which sheds light on the prototype design and motion control of the future underwater adhesion robot. Meanwhile, the obtained results offer some valuable insights into prolonging the endurance of underwater robots and constructing the mother–son multirobot system.

The rest of this article is organized as follows. The overall designs of the robotic remora and the adhesion system are provided in Section II. Section III describes the idea of the pose and depth controllers in detail. The experimental setup and the corresponding results are offered in Section IV. Finally, Section V concludes this article.

II. Mechatronic Design

The hitchhiking behavior of remora can usually be divided into three stages, namely, attaching to the host surface, following the host passively, and detaching from the host. To fulfill this hitchhiking task, the decoupled motion mechanism and the stable adhesion system are crucial in mechatronic design. On

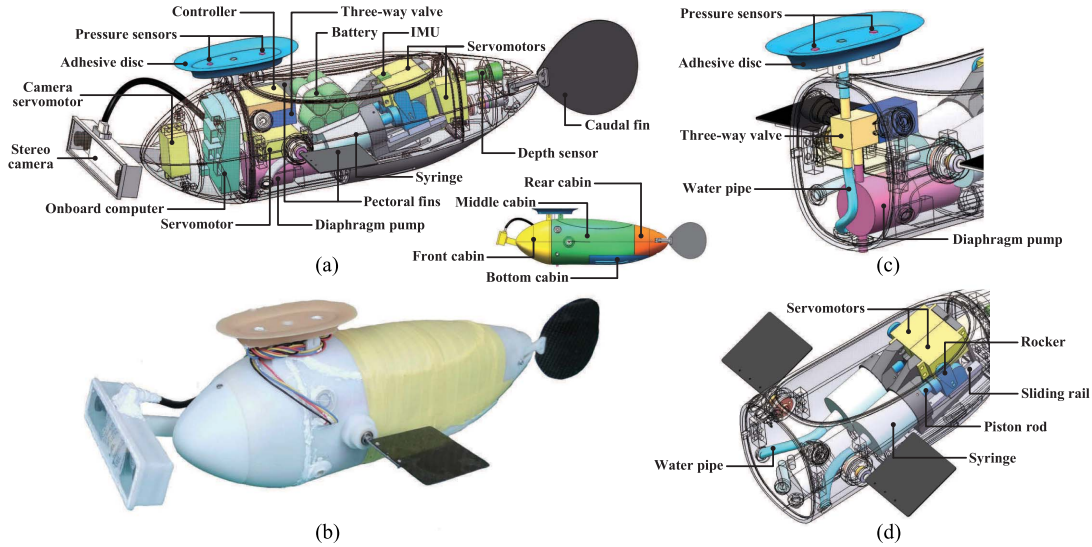

Fig. 2. Mechatronic design of the robotic remora. (a) Conceptual design. (b) Robotic prototype. (c) Adhesion system. (d) Buoyancy-driven system.

TABLE I
MECHATRONIC PARAMETERS OF THE DEVELOPED ROBOTIC REMORA

Items	Characteristics
Size ($L \times W \times H$)	$\sim 556 \times 222 \times 147$ mm^3
Total mass	~ 2860 g
Disc size ($L \times W \times H$)	$\sim 124 \times 70 \times 22$ mm^3
Disc mass	~ 50 g
Actuators	Servomotor×6 (pectoral fins×2, caudal fin×1, camera×1, buoyancy-driven system×2), diaphragm pump×1, three-way valve×1
Sensors	Stereo camera (Indemind), IMU (JY901), pressure sensors (MS5803), depth sensor (MS5837)
Communicators	Radio frequency devices (433 MHz)
Processors	STM32F407, Nvidia Jetson TX2
Power supply	Li-ion battery (DC 7.6 V / 11.4 V, 3200 mAh)

the one hand, motion decoupling, especially the independence on planar and vertical movement, can effectively simplify the controller design during the attaching stage. On the other hand, adhesion ability is the key feature of the remora; the adhesion system performance directly determines the success or failure of the hitchhiking task. Accordingly, this section introduces the mechatronic design around these two points.

A. Prototype Overview

The robot prototype inspired by the remora is shown in Fig. 2. The corresponding specifications are tabulated in Table I. From the appearance, this robotic remora consists of a well-streamlined rigid body, an adhesive disc, a caudal fin, a pair of pectoral fins, and a camera joint. The shell of the rigid body is made of resin material by 3-D printing technology. The adhesive disc is cast from silicone rubber by resin mold, which is mounted on the dorsum of robotic fish. The pectoral fins and caudal fin are fabricated from the flexible carbon fiber sheet with a thickness of 0.5 mm, which is beneficial for the motion performance.

The robotic remora consists of four parts, including the front, middle, rear, and bottom cabins. The front cabin is mounted with a visual system, including a stereo camera (Indemind), a camera servomotor, and an onboard computer (NVIDIA Jetson TX2) for processing visual data. The middle cabin carries the adhesion module [see Fig. 2(c)], two pectoral fin servomotors, two buoyancy-driven systems [see Fig. 2(d)], and a battery. The rear cabin equips with the tail joint, where the torque of servomotor is transmitted to the caudal fin through a set of bevel gears. The bottom cabin is applied to counter weight for improving the stability of the robot. The main control unit is the STM32F407, which undertakes the function of motion control, sensor data processing, and communication.

B. Motion System

To guarantee the independence of the planar and vertical motion, the robotic remora adopts the pectoral and caudal fins to achieve horizontal movement and the buoyancy-driven system to adjust the depth. The pectoral and caudal fins are driven by servomotors, and the range of motion of the pectoral joints is 360° and that of the tail joints is 120°. Owing to the higher thrust, the caudal fin is suitable for cruising on a large scale. Instead, pectoral fins can form various motion modes by mutual cooperation and, thus, are more appropriate for fine-tuning the robot pose in a small range. Fig. 3 depicts the available motion modes formed by a pair of pectoral fins, including forward, backward, upward movements, and differential steering. Furthermore, the locomotion of the fish fins is controlled by a central pattern generator (CPG) defined as follows [30]:

$$\begin{aligned} \dot{x}_i &= -f_i y_i + \mu_i (x_i - o_i)\left[a_i^2 - (x_i - o_i)^2 - y_i^2\right] \\ \dot{y}_i &= f_i (x_i - o_i) + \nu_i y_i \left[a_i^2 - (x_i - o_i)^2 - y_i^2\right] \\ \theta_i &= x_i \end{aligned} \tag{1}$$

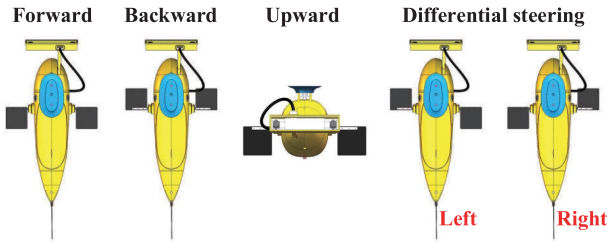

Fig. 3. Motion mode formed by a pair of pectoral fins.

where x_i and y_i denote the state variables of the ith oscillator, and θ_i is the output of the CPG controller, namely, the angle of joint. f_i, a_i, and o_i represent the oscillating frequency, amplitude, and offset, respectively. μ_i and ν_i are constants affecting the convergence speed of the oscillator. Subscripts $i = 1, 2, 3$ denote the left pectoral joint, right pectoral joint, and tail joint, respectively. Besides, in this article, the phase bias between the left and right pectoral fins is zero. The pectoral fins and caudal fin oscillate separately and without mutual inference.

Besides, as shown in Fig. 2(d), the buoyancy-driven systems are also driven by servomotors. The working principle is that the rotation of the rocker is converted into the rectilinear locomotion of piston rod by a sliding rail, so that the water volume in the syringe can be controlled to adjust the buoyancy.

C. Adhesion System

Adhesion system is the uppermost part of the overall robot. To realize a stable and reliable adhesion, several factors should be considered, including the requirements of preload, the magnitude of adhesive force and shear force, reversible adhesion ability, adhesion adaptability, and perceptual ability. Specifically, the larger preload forming adhesion requires, the lower the success rate of the adhesion is, especially for the underactuated robotic fish, which hardly provides a large force along a fixed direction. The maximal adhesive force and shear force decide the adhesion reliability. The reversible adhesion ability refers that the adhesion system can attach to and detach from the host repeatedly. The adhesion adaptability means that the suction disc can adhere to the flat surface with a range of inclination angles. Generally, when both the robotic fish and host are in suspension state, it is hardly possible for guaranteeing the adhesive disc parallel to the host surface during adhesion. Therefore, stronger adhesion adaptability can effectively increase the success rate of the adhesion. Finally, the perceptual ability is to fetch the adhesive state of the disc and avoid the failure of the adhesion.

In order to realize the characteristics of small preload and reversible adhesion, a novel adhesion system based on a diaphragm pump and a three-way solenoid valve is proposed [see Fig. 2(c)]. Note that when the valve is closed, the disc is connected with the pump through water pipe. By contrast, when the valve is open, the disc is directly connected with the external environment. Its working principles are as follows. In the attaching stage, the pump is turned ON and the valve is turned OFF. The water above the disc is pumped to the underneath of fish, which generates

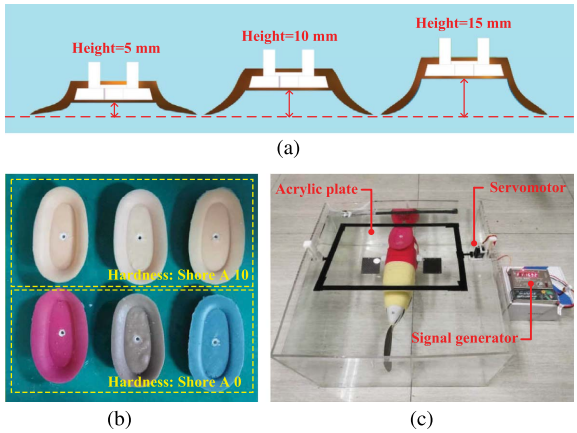

Fig. 4. Experimental setup of adhesive disc test. (a) Cross section of the discs with various heights. (b) Adhesive disc. (c) Adhesion adaptability test device.

an upward thrust. This impact and net buoyancy promote the disc to approach the host and finally form adhesion. For the attaching action, the only required preload is the net buoyancy, which is about 0.4 N. In detaching stage, the pump is turned OFF and the valve is turned ON, which destroys the negative pressure environment in the disc and thus breaks the adhesion. Besides, owing to the low power of both pump and valve (< 3 W) and short working time, the energy consumption of this adhesion system is negligible.

Apart from the small preload and reversible ability, the adhesive force, shear force, and the adhesion adaptability of disc should be further considered. These characteristics of disc are closely associated with the pump specification and the appearance and material of disc. In terms of the pump selection, the pump with a higher lift can maintain the larger negative pressure difference and, thus, produce the larger adhesive force and shear force. For the designed adhesion system, the pump is selected as a diaphragm pump with 2-m lift, which generates the maximum adhesive force over 250 N and the maximum shear force over 170 N. Considering that the robot mass is only 2.86 kg, the adhesive force can guarantee the stable adhesion even if the host is accelerated by about ten times gravity acceleration (ignoring fluid drag). Thus, the adhesive performance can fully satisfy the demand of use.

In the aspect of disc design, the adhesive force and shear force are affected by many factors. The main features of the adhesive disc, including the material hardness and disc height, are selected as research variables for investigating the basic rule about disc design. As shown in Fig. 4(a) and (b), we utilized the silicon rubber with two kinds of hardness (Shore A 0 and 10) to cast three suction discs with different heights, respectively. Fig. 5 shows the test results of these discs. In the force test, the disc was attached to a glass substrate firmly in water by applying a strong normal force. Then, the pull-off force and shear force were loaded at the disc via a string. Maximum adhesive and shear force were the highest value recorded between the start of a pull and the point at which the seal is broken. For the adhesion adaptability test, the experimental setup is shown in

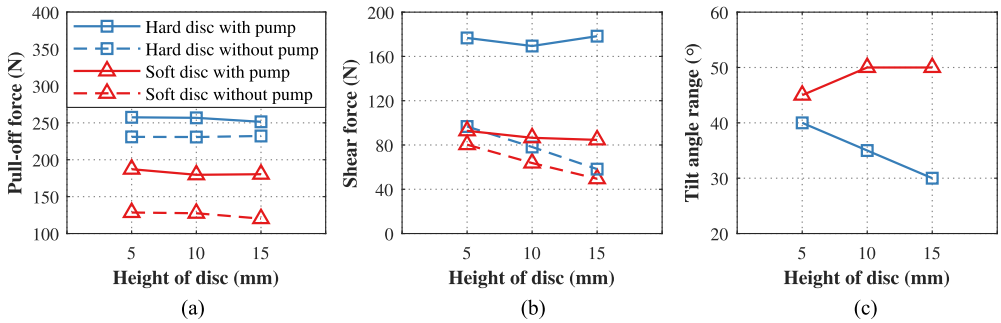

Fig. 5. Test results of the adhesive discs with various hardness (Shore A 0 and 10) and heights. (a) Maximum pull-off force test. (b) Maximum shear force test. (c) Adhesion adaptability test.

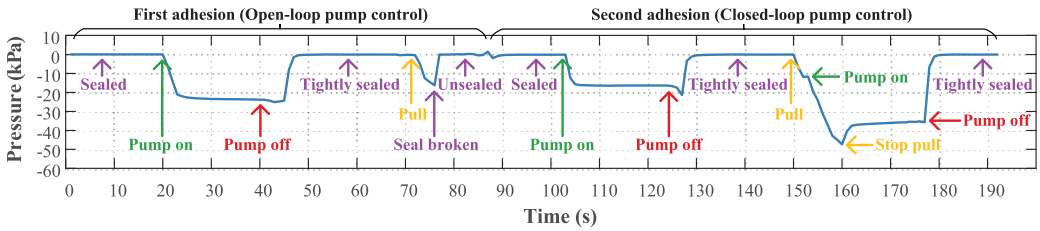

Fig. 6. Measured pressure in the interior of adhesive disc when a pull-off force is exerted.

Fig. 4(c). The tilt angle of the Acrylic plate was controlled by a servomotor, and a robotic remora equipping with a disc floated up to attach to the plate by net buoyancy and the suction of pump. The maximum angle range of the Acrylic plate at which the success rate of adhesion is larger than 60% was recorded. In light of these test results, the designed adhesive disc has satisfied the need of use. Furthermore, several conclusions favorable for the future disc design can be obtained as follows:

1) Pump can substantially improve the original adhesive force and shear force of disc.
2) The harder disc performs the larger adhesive force and shear force.
3) The disc height affects weakly the adhesive force but has a certain impact on the shear force. The higher disc, the smaller shear force.
4) The tilt angle range of flat board that can be attached to is larger for a soft disc.
5) For the hard disc, the larger height leads to the worse adhesion adaptability, but it is opposite for the soft disc.

Furthermore, for endowing the suction disc with the perceptual ability, two small-size pressure sensors are cast in the adhesive disc. The measured pressure reflects the adhesion state of disc and is capable to guide the pump operation. As shown in Fig. 6, the pressures in the interior of disc are measured when a pull-off force is exerted. Note that the atmospheric pressure has been deducted from the measured data. In the first adhesion, the pump was first turned ON for a while to create a tighter seal. Then, a pull-off force was exerted on the disc. After a short period of time, the seal was broken. However, in the second adhesion, the pump was turned ON again according to the pressure feedback, which prevented the pull-off force from breaking the adhesion. It implies that the perceptual ability of pressure can guarantee the adhesion reliability and improve the efficiency simultaneously. More specifically, the pump can be turned OFF when the pressure is stable and turned ON when the pressure decreases rapidly.

III. Motion Control

To realize the hitchhiking behavior, 3-D pose control that drives the robotic fish from one position to another position with a specific heading angle in the 3-D space is the critical technique. Benefiting from the rational mechanical design, the 3-D pose control of the proposed robotic remora can be divided into two fully independent control tasks, namely, planar pose control and depth control. This section gives the details of these two controllers.

A. Planar Pose Control

Planar pose control is a challenging problem for the bionic robotic fish. Generally, the robotic fish propelled by fins is a typical underactuated system, whose longitudinal and lateral motions are coupling and the brake mechanism is missed. For this system, the position and orientation control without consideration of velocity can be handled, but stopping at that pose precisely is quite challenging. Besides, compared with the caudal fin, a pair of 360° pectoral fins is more agile and conducive to the pose control task. Therefore, this subsection proposes a novel two-stage pectoral-fin-based pose control method, which includes the path-following stage and the fine adjustment stage. Note that only the oscillating amplitude of pectoral fins and swimming mode are control inputs, while the oscillating frequency is fixed at a suitable value.

Fig. 7 depicts the basic principle of the pose controller. The core task of the pose controller is to align the body frame of the

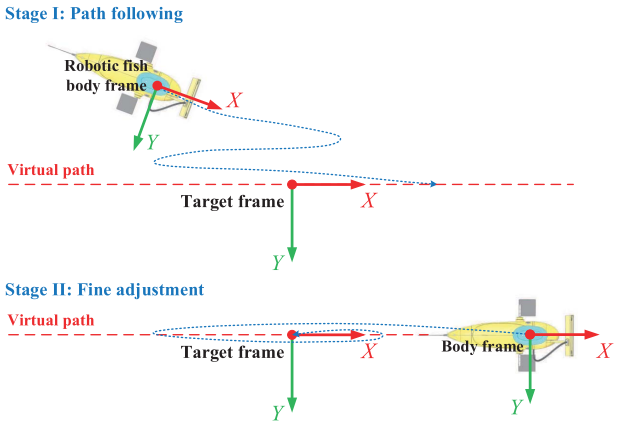

Fig. 7. Schematic of the two stages of the planar pose controller.

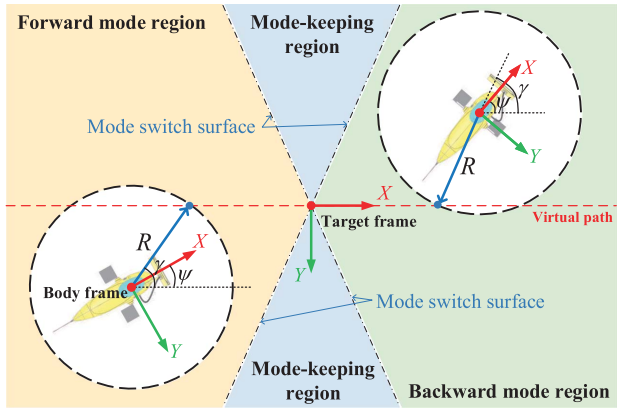

Fig. 8. Mode switch in path-following control.

robotic fish with the target frame. Since the pose of the robotic fish can be easily represented at the target frame, the pose control can be expressed as a regulation problem, which requires all the states, including position, heading angle, and velocity, to converge to the origin. To realize the control task, the robotic fish is first controlled to follow a virtual straight path, which is collinear with the x-axis of the target frame. When the lateral following error and heading error are lower than a threshold, the controller enters the next stage. In the fine adjustment stage, the robotic fish adjusts the longitudinal position and velocity along the virtual path and finally stops near the target point. In other words, the path-following stage realizes the convergence of the lateral position and the heading angle, while the fine adjustment further guarantees the longitudinal position and velocity return to zero. Besides, it is worth noting that the forward and backward motion modes of pectoral fins are switched repeatedly during the whole control process.

1) Path-Following Stage: Path-following control has been widely studied for robotic fish [31]. However, unlike the existing path-following methods, the continuous forward or backward motion is not permitted in this problem, since it will cause the robotic fish deviate from the target point and the sensors miss the target. Therefore, it is imperative to design a path-following controller with the mode-switch mechanism.

The idea of path following is shown in Fig. 8. The line-of-sight (LOS) guidance method is applied to transform the path-following control into the heading control [31]. To calculate the desired heading angle, a virtual circle with the radius R is put at the robotic fish position, and the intersection point between the virtual path and circle is applied to determine the desired orientation γ. For the forward and backward motion modes, the desired heading angle γ can be represented as

$$\gamma = \begin{cases} \arctan \frac{-Y}{\sqrt{R^2-Y^2}}, & \text{for forward mode} \\ \arctan \frac{Y}{\sqrt{R^2-Y^2}}, & \text{for backward mode} \end{cases} \tag{2}$$

where R is a predefined radius. X and Y denote the robot positions at target frame.

To realize the heading angle control, a PID control law is designed to adjust the oscillating amplitude of the pectoral fins, where the oscillating frequency is fixed at a suitable value. Owing to the characteristic of the fin propulsion, a pair of oscillating pectoral fins can generate the thrust and steering torque simultaneously. Accordingly, the oscillating amplitude of pectoral fins can be divided into two parts as follows:

$$\begin{bmatrix} A_{lp} \\ A_{rp} \end{bmatrix} = \begin{bmatrix} 1 & 1 \\ 1 & -1 \end{bmatrix} \begin{bmatrix} A_{\text{base}} \\ A_{\text{diff}} \end{bmatrix} \tag{3}$$

where A_{lp} and A_{rp} are the oscillating amplitudes of left and right pectoral fins, respectively. A_{base} denotes one part of amplitude that contributes to the thrust, and A_{diff} represents another part of amplitude that generates the steering torque.

Furthermore, in the path-following stage, the major consideration is the steering motion rather than the thrust or motion velocity of robotic fish. Thus, A_{base} is set as a constant, while A_{diff} is calculated by the following equation:

$$A_{\text{diff}} = \mathcal{S}(m)\left(k_{\psi p}\psi_e + k_{\psi d}\dot{\psi}_e + k_{\psi i}\int \psi_e dt\right) \tag{4}$$

where $\psi_e = \psi - \gamma$ denotes the heading angle error, and ψ is the heading angle. $k_{\psi p}$, $k_{\psi i}$, and $k_{\psi d}$ are the PID parameters. m denotes the current motion mode of robotic fish. $\mathcal{S}(m)$ distinguishes the control quantity between forward and backward modes. For example, the left steering motion in the forward mode requires large A_{rp} and small A_{lp}. But for the backward mode, A_{rp} should be smaller than A_{lp}. Thus, $\mathcal{S}(m)$ is defined as

$$\mathcal{S}(m) = \begin{cases} 1, & \text{if } m \text{ is forward mode} \\ -1, & \text{if } m \text{ is backward mode} \end{cases}.$$

Since the above control law depends on the current motion mode m, determining the motion mode of the robotic fish becomes a crucial problem to be addressed. The simplest way is swimming forward when $X < 0$ and swimming backward when $X > 0$. However, this strategy will lead to a high-frequency switching of motion mode and a low convergence speed of the following error. To avoid the high-frequency switching issue, a mode-keeping region is added, which is shown in Fig. 8. In the mode-keeping region, the robotic fish can hold the previous motion mode, namely, the motion mode when it enters this area, until it leaves. Fig. 9 shows the robot motion trajectories for various shapes of the mode-keeping region. Obviously, as shown

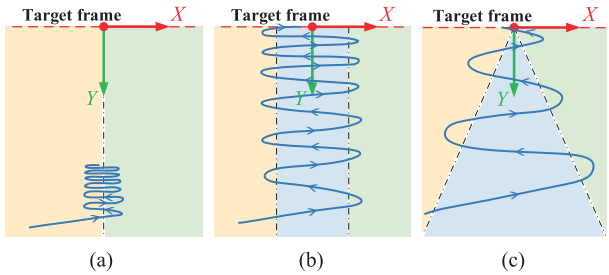

Fig. 9. Possible robot trajectories corresponding to the mode-keeping regions with various shapes. (a) Without mode-keeping region. (b) Rectangle mode-keeping region. (c) Triangle mode-keeping region.

in Fig. 9(b) and (c), the mode-keeping region should be wider with the increase in the lateral distance Y for improving the convergence speed. Thus, empirical definitions of the mode-keeping region, the forward mode region, and the backward mode region are as follows:

$$\begin{aligned}\mathcal{R}_{mk} &= \{(X,Y)|-k_m|Y|<X<k_m|Y|\}\\ \mathcal{R}_{fm} &= \{(X,Y)|X\le -k_m|Y|\}\\ \mathcal{R}_{bm} &= \{(X,Y)|X\ge k_m|Y|\}\end{aligned} \tag{5}$$

where $\mathcal{R}_{mk}$, $\mathcal{R}_{fm}$, and $\mathcal{R}_{bm}$ denote the corresponding planar regions for the mode-keeping, forward swimming, and backward swimming. $X=k_m|Y|$ and $X=-k_m|Y|$ are the equations of mode switch surface and $k_m\in\mathbb{R}$ is a constant. Note that this surface equation is not unique and can be selected freely.

2) Fine Adjustment Stage: When the robotic fish follows the path successfully, namely, $Y<\epsilon_1$ and $\psi_e<\epsilon_2$ (ϵ_1 and ϵ_2 are small constants), the pose control will enter the fine adjustment stage. The aim of this stage is to reduce the longitudinal position error and velocity and, meanwhile, keep following the path.

To ensure that the position and velocity of the robotic fish return to zero, one intuitive way is to decrease the thrust or oscillating amplitude with the decrement of longitudinal position error. The convergence of the thrust will finally lead to the convergence of velocity under the effect of fluid resistance. Besides, for path following, the control strategy of A_{diff} can still be adopted. Thus, the major difference for these two stages is the control law of A_{base}, which is designed as follows:

$$A_{\text{base}} = \mathcal{T}(d_e)A_p \tag{6}$$

where

$$d_e=\sqrt{X^2+Y^2},\ \mathcal{T}(x)=\frac{1-\exp(-k_v x)}{1+\exp(-k_v x)}$$

d_e is the position error, and A_p is a positive constant. $\mathcal{T}(x)$ is a monotonous decrease function, which is a dynamic gain of A_p and ensures that A_{base} is equal to zero when $d_e=0$. $k_v\in\mathbb{R}$ is an adjustable parameter. Note that $\mathcal{T}(x)$ is not unique and can be selected freely.

B. Depth Control

Depth control is a common task for the underwater robot, and thus, a wealth of methods have been proposed to address the issues existing in it. However, unlike the traditional underwater robots, the bionic robotic fish is propelled by the fin oscillation, which inevitably introduces the sinusoidal-like disturbance into the depth movement. Thus, disturbance attenuation is a vital issue to be discussed in the depth controller design of the robotic fish.

The depth dynamic of the proposed robotic remora with a buoyancy-driven system can be written as follows:

$$\begin{aligned}\dot{h} &= v_z\\ \dot{v}_z &= -\frac{k_z}{m_z}|v_z|v_z+\frac{\rho g S}{m_z}u_p+d\end{aligned} \tag{7}$$

where h and v_z are the depth and the vertical velocity, respectively. m_z is the sum of the mass and added mass in the vertical direction. k_z is a damping coefficient. ρ, g, and S are the water density, gravitational acceleration, and the cross-sectional area of the syringe, respectively. u_p is the displacement of piston rod, namely, control input. d represents the disturbance caused by the fin oscillation and water flow.

First, assuming $d=0$, the feedback linearization technique is applied to design a basic controller stabilizing the system without disturbance. Defining the desired depth as h_d and depth error as $e_h=h-h_d$, the basic controller is designed as

$$u_p=\frac{k_z}{\rho g S}|v_z|v_z+\frac{m_z}{\rho g S}(k_{hp}e_h+k_{hd}v_z) \tag{8}$$

where k_{hp} and k_{hd} are controller parameters.

Then, the error dynamic is as follows:

$$\begin{aligned}\dot{e}_h &= v_z\\ \dot{v}_z &= k_{hp}e_h+k_{hd}v_z\end{aligned} \tag{9}$$

where k_{hp} and k_{hd} can be easily designed to guarantee the convergence of the error dynamics.

Furthermore, a nonlinear disturbance observer (NDOB) is designed to estimate and compensate the lumped disturbance [32]. Define an auxiliary variable

$$z=\hat{d}-p(v_z) \tag{10}$$

where $\hat{d}$ is the estimation of disturbance and $p(v_z)$ is a function to be designed. The formulation of a NDOB can be written as

$$\begin{aligned}\dot{z} &= -l(v_z)z-l(v_z)\left[-\frac{k_z}{m_z}|v_z|v_z+\frac{\rho g S}{m_z}u+p(v_z)\right]\\ \hat{d} &= z+p(v_z)\end{aligned} \tag{11}$$

where $l(v_z)$ is the observer gain that satisfies the relationship of $l(v_z)=\partial p(v_z)/\partial v_z$. In this case, the observer error equation becomes

$$\dot{e}_d=-l(v_z)e_d \tag{12}$$

where $e_d=d-\hat{d}$ is the disturbance estimation error. To ensure that observer error dynamic is asymptotically stable regardless of v_z, the observer gain $l(v_z)$ is chosen as c and $c>0$. Then, $p(v_z)$ can be calculated as cv_z, and the complete NDOB equations for

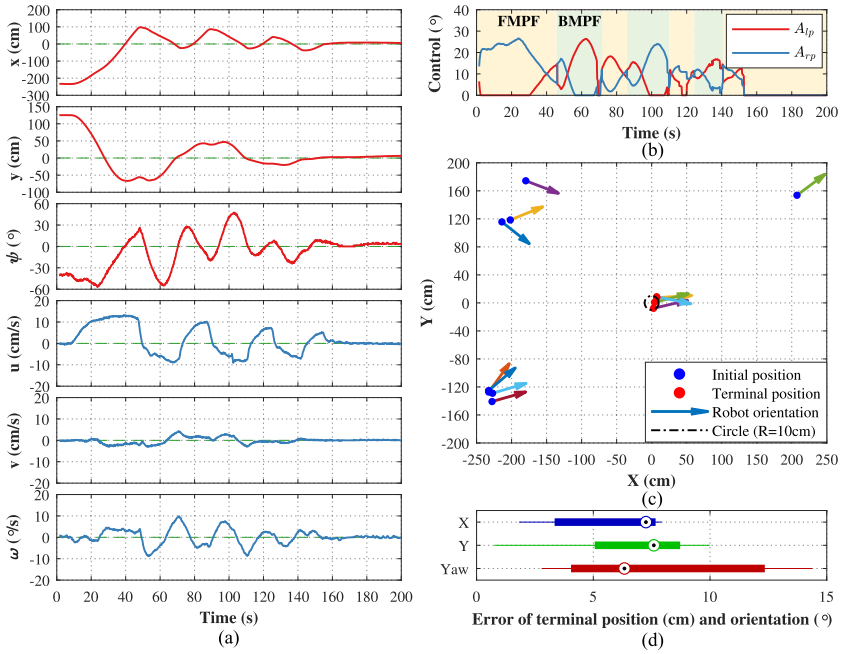

Fig. 10. Experimental results of planar pose control. (a) State curves of a typical experiment (x, y, u, and v represent the positions and velocities of the x-axis and y-axis, respectively. ψ and ω are the heading angle and angular velocity.). (b) Control curve of a typical experiment. (c) Eight experiments with various initial pose. (b) Boxplot of the terminal pose error for these eight experiments.

the system (7) are as follows:

$$\dot{z} = -cz + c\frac{k_z}{m_z}|v_z|v_z - c\frac{\rho g S}{m_z}u - c^2 v_z$$
$$\hat{d} = z + cv_z. \tag{13}$$

Finally, the estimated disturbance is substituted into the control law to restrain the disturbance

$$u_p = \frac{k_z}{\rho g S}|v_z|v_z + \frac{m_z}{\rho g S}(k_{hp}e_h + k_{hd}v_z) - \frac{m_z}{\rho g S}\hat{d}. \tag{14}$$

IV. Experiments

In order to evaluate the performance of the designed robotic remora and the effectiveness of the proposed control method, a number of experiments were conducted, including the pose control test, depth control test, and hitchhiking experiment. All experiments were performed in a 500 cm × 400 cm × 150 cm pool. Besides, an online global vision tracking system is equipped above the pool to collect the motion data, including the robot position and heading angle, and then provide feedback.

A. Pose Control Experiment

To validate the effectiveness of the proposed control method, the pose control experiments were conducted at an indoor pool. The position and heading angle of robotic fish were measured by the global vision tracking system in real time, and the feedback frequency was 8 Hz. Besides, the oscillating frequency of pectoral fin was set at 2 Hz. The upper bound of oscillating amplitude was 30°. The radius of the LOS method was 100 cm. The mode switch equations were selected as $X = 10 + |Y|$ and $X = -10 - |Y|$.

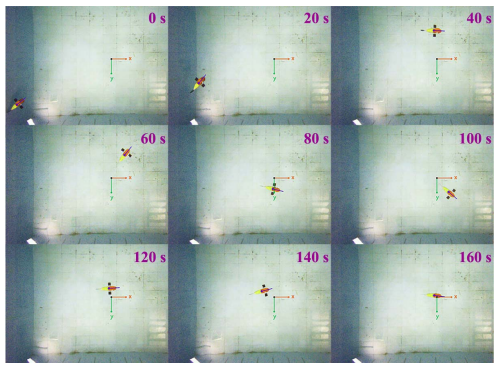

Fig. 11. Snapshot sequences of planar pose control.

The experimental results are shown in Fig. 10. Typically, Fig. 10(a) shows the state curves of one experiment. All states converge to a small neighborhood of origin after a period of adjustment. Furthermore, the convergence trend of position and velocity curve is apparent, but the change of heading angle is irregular. A possible reason for this is the asymmetry of the left and right steering mobility, which leads to a discrepancy in left and right steering movements even if the control input is symmetrical. Besides, an extra deceleration behavior that the pectoral fins are set at an upright position for increasing the water drag is utilized when the position error is small. Owing to this mechanism, the velocity rapidly reduces to zero without overshoot at about 160 s. Fig. 10(b) shows the corresponding control curve. It can be easily seen that the complete control process has gone through several mode switches between the forward mode of pectoral fin (FMPF) and backward mode of pectoral fin (BMPF), and then, the control quantity reduces to zero gradually. Fig. 11 shows the snapshot sequences of the experiment, which are captured by the global camera.

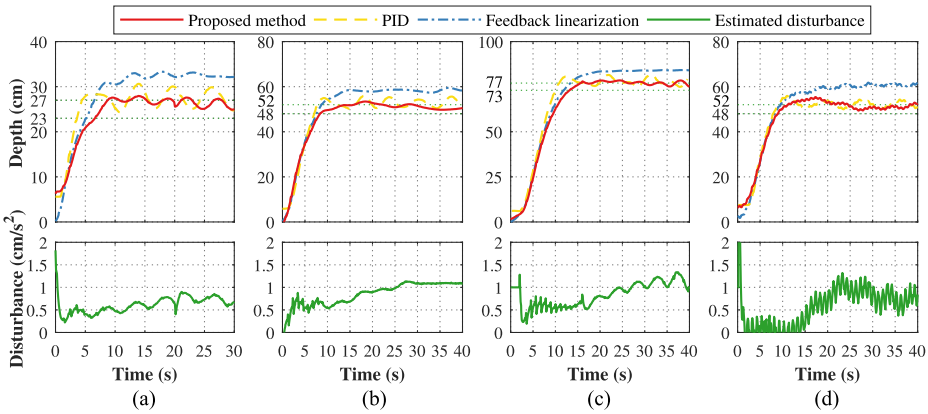

Fig. 12. Comparative experiment results of depth control. (a)–(c) Static condition ($h_d = 25,\ 50,\ 75$ cm). (d) Dynamic condition ($h_d = 50$ cm, pectoral fin forward mode, frequency: 1 Hz, amplitude: 40°).

Fig. 10(c) shows the results of eight pose control experiments. The robotic fish starts at various poses and finally returns to origin. It can be seen that all robotic fishes arrive and stop at a 10-cm area around the origin, and their heading angles are near zero. Fig. 10(d) depicts the detailed statistical results about control error. The X and Y position errors are lower than 10 cm. The maximum error of heading angle is 14.37°, but the median of heading angle error is 6.54°.

In a word, the repeated pose control experiments demonstrate that the effectiveness and robustness of the proposed method in practical application, which lays a foundation for the adhesion behavior.

B. Depth Control Experiment

For demonstrating the effectiveness of the proposed depth controller, a series of comparative experiments about various controllers, including PID and feedback linearization controllers, were conducted under static and dynamic conditions. Note that the depth data were measured by the depth sensor. To exhibit the anti-interference ability of our method, the net buoyancy of the robotic remora was set to be slightly smaller than zero, which implies that the robot will sink when the control input is zero. Note that this experiment setting is rational since the net buoyancy hardly equals absolute zero in practice.

The experimental results are shown in Fig. 12. With regard to the transient stage, the rise time and response speed are quite similar for these three methods. However, the control performance differences of them are significant in the steady stage owing to the constant disturbance induced by the nonzero net buoyancy. The feedback linearization method has hardly any fluctuation but an obvious steady-state error. The PID method possesses a smaller steady-state error but an evident fluctuation. The proposed method maintains the depth error in a range of ±2 cm with a gentle fluctuation, which exhibits the superior disturbance attenuation ability. Furthermore, the estimated disturbances are almost consistent in four experiments, which fluctuate between 0.5 and 1.5 cm/s^2. It reveals that the proposed disturbance observer can effectively estimate the unknown disturbance. Besides, Fig. 13 shows the movement of robotic fish during the depth control.

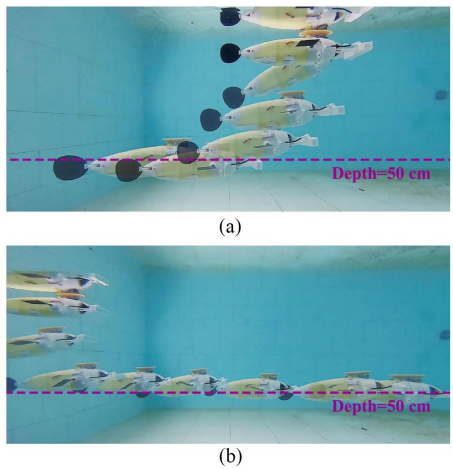

Fig. 13. Snapshots of depth control. (a) Static condition. (b) Dynamic condition (pectoral fin forward mode).

In conclusion, the designed depth controller possesses superior performance on both static and dynamic cases, which paves the way for hitchhiking control.

C. Hitchhiking Experiment

To validate the motion ability and adhesion function of the proposed system, a complete hitchhiking experiment was carried out by the robotic remora through remote control. Note that the robot depth was automatically controlled by the proposed depth controller, and the target depth was allocated manually. In addition, the five motion modes exhibited in Fig. 3 were utilized to control the position and attitude of the robotic remora by hand in the hitchhiking process.

As shown in Fig. 14, the complete hitchhiking behavior consists of three stages. In the attaching stage, the robotic remora finely adjusted the position and heading angle by a pair of pectoral fins and finally adhered to the host with the cooperation of depth control. In the following stage, the adhesion system exhibited a considerable pull-off force and shear force, which prevent the high maneuver of the host to break adhesion. In the detaching stage, the robotic remora fell off the

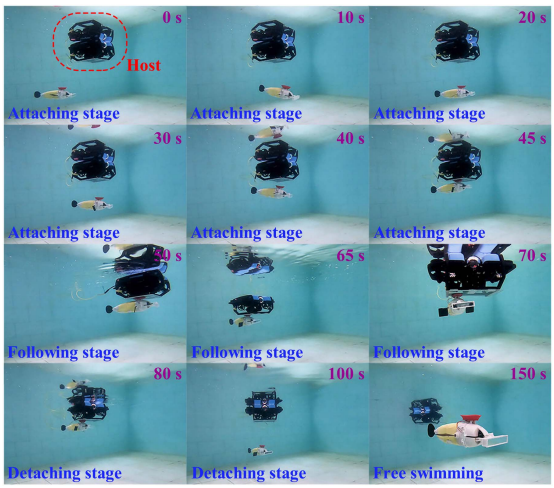

Fig. 14. Snapshot sequences of the complete hitchhiking behavior of robotic remora.

host in a short duration with no need of external assistance. In conclusion, the hitchhiking experiment validates the flexible mobility and complete adhesion function of the proposed robotic remora.

D. Discussion

As the experimental results show, the proposed robotic remora possesses agile mobility as well as a reliable and adaptable adhesion system. In particular, compared with the previous works, the designed adhesion system only requires a small preload, namely, net buoyancy, which makes it possible for the practical adhesion application on the robotic fish. Besides, the combination of pump and valve ensures enough adhesive and shear forces and realizes the function of reversible adhesion. The pressure sensor is cast in the adhesive disc to accomplish the feedback control of adhesion, which further strengthens the practicability of disc.

Furthermore, the mode-switch-based planar pose control method implements the regulation and station-keeping of both position and orientation for the robotic fish, which is rarely reported in previous works. As the pose control method only involves the basic motion rather than the dynamic of the robotic fish, the idea of two-stage control and mode-switch mechanism can be used for other underwater robots with the ability of forward, backward, and steering movement. Besides, the proposed antidisturbance depth control method can compensate for the disturbance effectively, especially the constant interference caused by the nonzero net buoyancy. In addition, this depth controller is based on the buoyancy-driven mechanism and the universal fluid drag model, which can be applied to most of the underwater robots equipped with a buoyancy-driven system. In general, the design of these two controllers is dominated by practicability, which is sufficiently validated by extensive experiments.

However, despite the successful implementation of the designed system, there is still room for improvement. For instance, the wire-driven mechanism or the pneumatic actuator can be adopted to increase the freedom of motion of disc so that it can adhere to the surface with various inclination angles. Besides, the flexible pressure sensor can be cast in the soft lip of disc so that the accurate contact position can be perceived, which is conducive for more intelligent adhesion.

V. Conclusion

In this article, we have successfully implemented the hitchhiking behavior of remora in the engineered system, which benefits from the agile robotic prototype, reliable adhesion system, as well as the precise and robust control methods. To guarantee the mobility of the robot, the independent planar and vertical motion mechanisms are introduced in the robotic remora, especially a pair of highly flexible pectoral fins and buoyancy-driven systems. Then, aiming to the low preload demand, large adhesive force, reversible adhesion, and perceptual ability, the adhesion system is developed. Furthermore, a mode-switch-based planar pose controller and an antidisturbance depth controller are proposed to realize precise and stable station-keeping so that the robotic remora adheres to the host. Finally, the performance of the robot and adhesion system and the validity of the control methods are evaluated with experimental results. Such results will provide valuable insights into the future design of the robotic fish with long endurance and the mother–son multirobot system.

The ongoing and future work will focus on enhancing the underwater perception ability of the robotic fish to realize the autonomous hitchhiking behavior.

References

[1] R. Wang, S. Wang, Y. Wang, L. Cheng, and M. Tan, "Development and motion control of biomimetic underwater robots: A survey," *IEEE Trans. Syst., Man, Cybern., Syst.*, early access, doi: 10.1109/TSMC.2020.3004862.

[2] F. Zhang, J. Thon, C. Thon, and X. Tan, "Miniature underwater glider: Design and experimental results," *IEEE/ASME Trans. Mechatronics*, vol. 19, no. 1, pp. 394–399, Feb. 2014.

[3] P. Phamduy, J. Cheong, and M. Porfiri, "An autonomous charging system for a robotic fish," *IEEE/ASME Trans. Mechatronics*, vol. 21, no. 6, pp. 2953–2963, Dec. 2016.

[4] H. Dong, Z. Wu, D. Chen, M. Tan, and J. Yu, "Development of a whale-shark-inspired gliding robotic fish with high maneuverability," *IEEE/ASME Trans. Mechatronics*, vol. 25, no. 6, pp. 2824–2834, Dec. 2020.

[5] B. E. Flammang *et al.*, "Remoras pick where they stick on blue whales," *J. Exp. Biol.*, vol. 223, no. 20, 2020, Art. no. jeb226654.

[6] J. F. Steffensen and J. P. Lomholt, "Energetic cost of active branchial ventilation in the sharksucker, Echeneis naucrates," *J. Exp. Biol.*, vol. 103, no. 1, pp. 185–192, 1983.

[7] K. Autumn *et al.*, "Adhesive force of a single gecko foot-hair," *Nature*, vol. 405, no. 6787, pp. 681–685, 2000.

[8] W. M. Kier and A. M. Smith, "The structure and adhesive mechanism of octopus suckers," *Integr. Comparative Biol.*, vol. 42, no. 6, pp. 1146–1153, 2002.

[9] D. K. Wainwright, K. Thomas, K. Anja, N. G. Stanislav, and P. A. Adam, "Stick tight: Suction adhesion on irregular surfaces in the northern clingfish," *Biol. Lett.*, vol. 9, no. 3, 2013, Art. no. 20130234.

[10] B. A. Fulcher and P. J. Motta, "Suction disk performance of Echeneid fishes," *Can. J. Zool.*, vol. 84, no. 1, pp. 42–50, 2006.

[11] F. Tramacere, M. Follador, N. M. Pugno, and B. Mazzolai, "Octopus-like suction cups: From natural to artificial solutions," *Bioinspir. Biomim.*, vol. 10, no. 3, 2015, Art. no. 035004.

[12] A. Sadeghi, L. Beccai, and B. Mazzolai, "Design and development of innovative adhesive suckers inspired by the tube feet of sea urchins," in *Proc. Int. Conf. Biomed. Robot. Biomechatronics*, Rome, Italy, Jun. 2012, pp. 617–622.

[13] J. A. Sandoval, S. Jadhav, H. Quan, D. D. Deheyn, and M. T. Michael, "Reversible adhesion to rough surfaces both in and out of water, inspired by the clingfish suction disc," *Bioinspir. Biomim.*, vol. 14, no. 6, 2019, Art. no. 066016.

[14] Y. Wang *et al.*, "A biorobotic adhesive disc for underwater hitchhiking inspired by the remora suckerfish," *Sci. Robot.*, vol. 2, no. 10, 2017, Art. no. eaan8072.
[15] S. Wang *et al.*, "Detachment of the remora suckerfish disc: Kinematics and a bio-inspired robotic model," *Bioinspir. Biomim.*, vol. 15, no. 5, 2020, Art. no. 056018.
[16] K. M. Gamel, A. M. Garner, and B. E. Flammang, "Bioinspired remora adhesive disc offers insight into evolution," *Bioinspir. Biomim.*, vol. 14, no. 5, 2019, Art. no. 056014.
[17] S. H. Lee, H. W. Song, B. S. Kang, and M. K. Kwak, "Remora-inspired reversible adhesive for underwater applications," *ACS Appl. Mater. Interfaces*, vol. 11, no. 50, pp. 47571–47576, 2019.
[18] L. Li *et al.*, "Bottom-level motion control for robotic fish to swim in groups: Modeling and experiments," *Bioinspir. Biomim.*, vol. 14, no. 4, 2019, Art. no. 046001.
[19] S. Chen, J. Wang, and X. Tan, "Backstepping-based hybrid target tracking control for a carangiform robotic fish," in *Proc. Dyn. Syst. Control Conf.*, Palo Alto, CA, USA, Oct. 2013, vol. 56130, Art. no. V002T32A005.
[20] J. Yu, M. Tan, S. Wang, and E. Chen, "Development of a biomimetic robotic fish and its control algorithm," *IEEE Trans. Syst., Man, Cybern., Cybern.*, vol. 34, no. 4, pp. 1798–1810, Aug. 2004.
[21] K. Zou, C. Wang, G. Xie, T. Chu, L. Wang, and Y. Jia, "Cooperative control for trajectory tracking of robotic fish," in *Proc. Amer. Control Conf.*, St Louis, MO, USA, Jun. 2009, pp. 5504–5509.
[22] N. Kato, "Control performance in the horizontal plane of a fish robot with mechanical pectoral fins," *IEEE J. Ocean. Eng.*, vol. 25, no. 1, pp. 121–129, Jan. 2000.
[23] P. Zhang, Z. Wu, Y. Meng, M. Tan, and J. Yu, "Nonlinear model predictive position control for a tail-actuated robotic fish," *Nonlinear Dyn.*, vol. 101, no. 4, pp. 2235–2247, 2020.
[24] J. Yu, F. Sun, D. Xu, and M. Tan, "Embedded vision-guided 3-D tracking control for robotic fish," *IEEE Trans. Ind. Electron.*, vol. 63, no. 1, pp. 355–363, Jan. 2016.
[25] J. Yu, J. Liu, Z. Wu, and H. Fang, "Depth control of a bioinspired robotic dolphin based on sliding mode fuzzy control method," *IEEE Trans. Ind. Electron.*, vol. 65, no. 3, pp. 2429–2438, Mar. 2018.
[26] F. Shen, Z. Gao, C. Zhou, D. Xu, and N. Gu, "Depth control for robotic dolphin based on fuzzy PID control," *Int. J. Offshore Polar Eng.*, vol. 23, no. 3, pp. 166–171, 2013.
[27] R. K. Katzschmann, J. DelPreto, R. MacCurdy, and R. Daniela, "Exploration of underwater life with an acoustically controlled soft robotic fish," *Sci. Robot.*, vol. 3, no. 16, 2018, Art. no. eaar3449.
[28] J. Wang, Z. Wu, M. Tan, and J. Yu, "Model predictive control-based depth control in gliding motion of a gliding robotic dolphin," *IEEE Trans. Syst., Man, Cybern., Syst.*, vol. 51, no. 9, pp. 5466–5477, Sep. 2021.
[29] M. Makrodimitris, I. Aliprantis, and E. Papadopoulos, "Design and implementation of a low cost, pump-based, depth control of a small robotic fish," in *Proc. IEEE/RSJ Int. Conf. Intell. Robot. Syst.*, Chicago, IL, USA, Sep. 2014, pp. 1127–1132.
[30] J. Yu, Z. Wu, M. Wang, and M. Tan, "CPG network optimization for a biomimetic robotic fish via PSO," *IEEE Trans. Neural Netw. Learn. Syst.*, vol. 27, no. 9, pp. 1962–1968, Sep. 2016.
[31] J. Liu, Z. Wu, J. Yu, and M. Tan, "Sliding mode fuzzy control-based path-following control for a dolphin robot," *Sci. China Inf. Sci.*, vol. 61, no. 2, 2018, Art. no. 024201.
[32] W. Chen, J. Yang, L. Guo, and S. Li, "Disturbance-observer-based control and related methods—An overview," *IEEE Trans. Ind. Electron.*, vol. 63, no. 2, pp. 1083–1095, Feb. 2016.

Pengfei Zhang received the B.E. degree in detection, guidance, and control techniques from the School of Aeronautics and Astronautics, Central South University, Changsha, China, in 2017. He is currently working toward the Ph.D. degree in control theory and control engineering with the Institute of Automation, Chinese Academy of Sciences, Beijing, China.

His research interests include the intelligent control and environmental perception of bioinspired robotic fish.

Zhengxing Wu received the B.E. degree in logistics engineering from the School of Control Science and Engineering, Shandong University, Jinan, China, in 2008, and the Ph.D. degree in control theory and control engineering from the Institute of Automation, Chinese Academy of Sciences (IACAS), Beijing, China, in 2015.

He is currently a Professor with the State Key Laboratory of Management and Control for Complex Systems, IACAS. His research interests include fast maneuvers of bioinspired robotic fish and gliding motions of robotic dolphins.

Yan Meng received the B.E. degree in mechanical engineering from the School of Mechanical Engineering, University of Science and Technology Beijing, Beijing, China, in 2017. He is currently working toward the Ph.D. degree in control theory and control engineering with the Institute of Automation, Chinese Academy of Sciences.

His current research interests include robotic fish and intelligent control systems.

Huijie Dong received the B.E. degree in automation from the University of Shanghai for Science and Technology, Shanghai, China, in 2013, and the M.E. degree in control science and engineering from the Taiyuan University of Technology, Taiyuan, China, in 2018. He is currently working toward the Ph.D. degree in control theory and control engineering with the Institute of Automation, Chinese Academy of Sciences, Beijing, China.

His current research interests include bioinspired underwater robots and intelligent control systems.

Min Tan received the B.Sc. degree from Tsinghua University, Beijing, China, in 1986, and the Ph.D. degree from the Institute of Automation, Chinese Academy of Sciences (IACAS), Beijing, in 1990, both in control science and engineering.

He is currently a Professor with the State Key Laboratory of Management and Control for Complex Systems, IACAS. He has authored or coauthored more than 200 papers in journals, books, and conference proceedings.

His research interests include robotics and intelligent control systems.

Junzhi Yu (Fellow, IEEE) received the B.E. degree in safety engineering and the M.E. degree in precision instruments and mechanology from the North University of China, Taiyuan, China, in 1998 and 2001, respectively, and the Ph.D. degree in control theory and control engineering from the Institute of Automation, Chinese Academy of Sciences, Beijing, China, in 2003.

From 2004 to 2006, he was a Postdoctoral Research Fellow with the Center for Systems and Control, Peking University, Beijing. In 2006, he was an Associate Professor with the Institute of Automation, Chinese Academy of Sciences, where he was a Full Professor in 2012. In 2018, he joined the College of Engineering, Peking University, as a Tenured Full Professor. His current research interests include intelligent robots, motion control, and intelligent mechatronic systems.